



This is a repository copy of *A hybrid battery parameter identification concept for lithium-ion energy storage applications*.

White Rose Research Online URL for this paper:

<http://eprints.whiterose.ac.uk/113906/>

Version: Accepted Version

Proceedings Paper:

Nejad, S., Gladwin, D.T. orcid.org/0000-0001-7195-5435 and Stone, D.A. orcid.org/0000-0002-5770-3917 (2016) A hybrid battery parameter identification concept for lithium-ion energy storage applications. In: IECON Proceedings (Industrial Electronics Conference). IECON 2016 - 42nd Annual Conference of the IEEE Industrial Electronics Society, October 24-27, 2016, Florence. , pp. 1980-1985. ISBN 9781509034741

<https://doi.org/10.1109/IECON.2016.7793233>

Reuse

Unless indicated otherwise, fulltext items are protected by copyright with all rights reserved. The copyright exception in section 29 of the Copyright, Designs and Patents Act 1988 allows the making of a single copy solely for the purpose of non-commercial research or private study within the limits of fair dealing. The publisher or other rights-holder may allow further reproduction and re-use of this version - refer to the White Rose Research Online record for this item. Where records identify the publisher as the copyright holder, users can verify any specific terms of use on the publisher's website.

Takedown

If you consider content in White Rose Research Online to be in breach of UK law, please notify us by emailing eprints@whiterose.ac.uk including the URL of the record and the reason for the withdrawal request.

A Hybrid Battery Parameter Identification Concept For Lithium-ion Energy Storage Applications

S.Nejad, D. T. Gladwin and D. A. Stone

Department of Electronic and Electrical Engineering
University of Sheffield
Sheffield, United Kingdom
S.Nejad@Sheffield.ac.uk

Abstract—Persistent of excitation of the input/output signals is a necessity for any online parameter identification technique. In most real battery systems, the drive signals may not fully satisfy this condition at all times, which can lead to divergence and failure of the incorporated battery management system. Therefore, in this paper, a hybrid battery parameter identification concept is proposed whereby the parameters are initially identified using a special random signal called the pseudo random binary sequences. Thereafter, the Kalman filter algorithm is implemented online to estimate and track any ‘disturbances’ caused by varying operating conditions. A dynamic European drive cycle is used to experimentally verify the excellent performance of the proposed technique against a more precise electrochemical impedance spectroscopy method.

Keywords—Lithium-ion; Battery Energy Storage; Online; Extended Kalman Filter; Hybrid; Parameter Identification;

I. INTRODUCTION

Lithium-ion batteries have been extensively used for electrical energy storage and supply in a variety of applications. These range from low-power (milli Watts) portable electronic devices to high-power (kilo Watts) electric vehicles (EVs) and recently emerged super-power (mega Watts) grid-tie applications. Regardless of the intended use, a battery management system (BMS) must be put in place to maintain a safe battery operating envelope for both consumer convenience and prolongation of the battery’s lifetime. Typical tasks performed by a modern BMS, as depicted in Fig. 1, include the estimation of the battery’s state-of-charge (SOC) state-of-power (SOP) and state-of-function (SOF).

In order to accurately estimate these states in real time, modern BMSs often use dynamic model representations of the battery under operation. Various model structures have been presented in literature, of which those lumped-parameter equivalent-circuit models are found most popular. For most *in situ* applications, such as in EVs and grid-tie storage, the battery model parameters need to be identified in real time. In the past, researchers have implemented different techniques such as the moving-window least-squares method [1] and the dual Extended Kalman Filter (DEKF) [2], [3] to identify and adapt the battery model parameters in real time.

In [4] we reported that the battery model parameters vary with SOC and thus with time. Due to this time-variability of the model parameters, the input/output signals must be persistently exciting to a certain order [5]. This pre-condition is

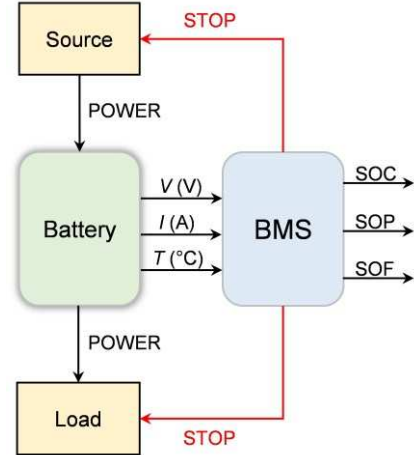


Fig. 1. Overview of typical tasks performed by a BMS

a necessity for any online parameter identification technique to be able to properly reveal the contents of battery dynamics. However, in many real battery systems (e.g. in EVs), the current signal may not be sufficiently exciting at all times. In practice, the dual-EKF algorithm as opposed to those observer-based estimators (e.g. Luenberger observer) seems to operate well without any divergence. This is true if and only if *a priori* knowledge of the model parameters are available at the initialisation step [5]. When dealing with non-linear systems, even a small error in the initial conditions can cause a large deviation in the estimated quantity.

Therefore, in this paper, a hybrid battery parameterisation technique is proposed based on the pseudo random binary sequences (PRBS) to provide the DEKF algorithm with a reasonable prior knowledge of the system to be identified. The battery is required to be in open-circuit mode for at least thirty minutes prior to PRBS characterisation to ensure a steady-state condition is partially realised. Thereafter, upon the load engagement, the DEKF algorithm is applied online to effectively deal with the ‘disturbances’ caused in the battery parameters by the external stress factors such as variations in ambient temperature, ageing and SOC modification.

II. EXPERIMENTAL SETUP

In order to verify the proposed method, a number of tests are performed on a 3.6 Ah lithium-ion nickel manganese cobalt oxide (NMC) cylindrical cell. The experimental configuration,

as illustrated in Fig. 2, features a multi-channel Maccor 4000-series battery tester with voltage and current measurement accuracies of $\pm 0.02\%$ and $\pm 0.05\%$ of the full scale range respectively. The ambient temperature is controlled through a built-in-house thermal chamber with ± 1 °C accuracy. A desktop computer is used to provide software control and data storage for later analysis. Since the current sensor noise of the Maccor system is relatively small and the sampling rate is reasonably high ($T_s = 10$ ms), it is safe to assume that the integral of the throughput current over the charge/discharge period represents a ‘true’ measurement of SOC. Finally, a Solartron 1260 electrochemical interface is used in conjunction with a Solartron 1287 frequency response analyser to perform a series of electrochemical impedance spectroscopy (EIS) tests. The complex impedance data obtained from the EIS tests will be used to verify the accuracy of the PRBS identification method.

III. DYNAMIC MODEL DESCRIPTION

A. Lumped-Parameter Equivalent-Circuit Model

Due to their simplified structures, equivalent electrical-circuit battery models (e.g. Randles’ model [6], [7]) are often used in real-time battery power management problems. In general, as depicted in Fig. 3, these models are comprised of an ideal voltage source that represents the battery/cell’s open-circuit voltage (OCV) as a function of SOC and possibly temperature and a resistor R_s in series with n number of series-connected parallel resistor-capacitor (RC) branches.

Considering the model structure given in Fig. 3, the battery’s output voltage V_k in discrete time can be written as the following set of linear time-varying (LTV) equations,

$$\begin{bmatrix} V_{RCn_{k+1}} \\ \vdots \\ V_{RC1_{k+1}} \end{bmatrix} = \begin{bmatrix} -T_s \\ e^{\frac{-T_s}{R_1 C_1}} & \dots & 0 \\ \vdots & \ddots & \vdots \\ 0 & \dots & e^{\frac{-T_s}{R_n C_n}} \end{bmatrix} \begin{bmatrix} V_{RC1_k} \\ \vdots \\ V_{RCn_k} \end{bmatrix} + \begin{bmatrix} R_1 \left(1 - e^{\frac{-T_s}{R_1 C_1}}\right) & \dots & 0 \\ \vdots & \ddots & \vdots \\ 0 & \dots & R_n \left(1 - e^{\frac{-T_s}{R_n C_n}}\right) \end{bmatrix} I_k \quad (1)$$

$$V_k = V_{OC}(SOC_k) - V_{RC1_k} - \dots - V_{RCn_k} - I_k R_s \quad (2)$$

$$SOC_{k+1} = SOC_k - \frac{\eta I_k T_s}{3600 \times C_{Ah}} \quad (2)$$

where V_{RC1} to V_{RCn} are the transient voltages, T_s is the sampling period, η is the battery’s coulombic efficiency, I_k is the throughput current and C_{Ah} is battery capacity in ampere-hours. In this case, $T_s = 10$ ms and $\eta = 0.99$.

Depending on the dynamics of the intended application, the number of RC branches can vary. However, for most applications involving high-power lithium-ion batteries, one or

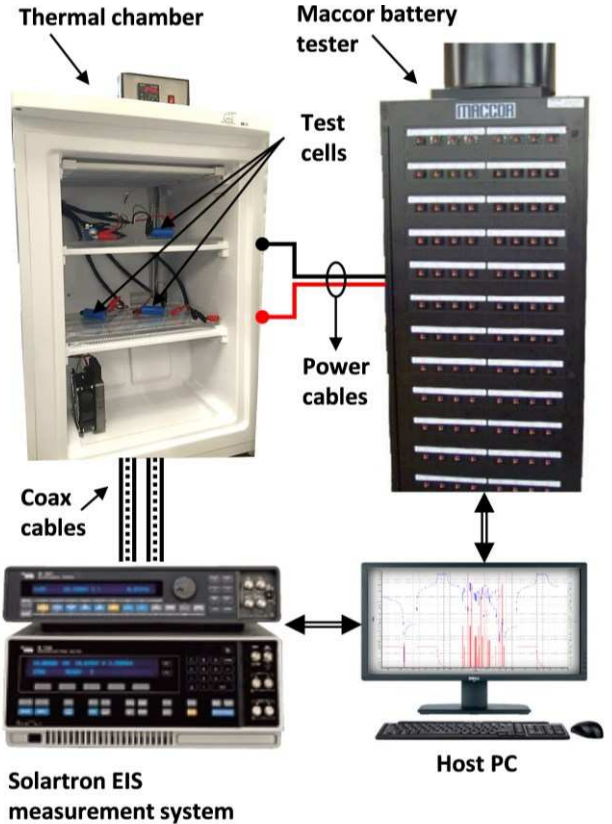


Fig. 2. Experimental setup, showing hardware configuration

two RC branches often suffice the modelling requirements in terms of complexity and accuracy. In this work, a two time-constant model structure (i.e. $n = 2$) is chosen, where one RC branch represents the short time-constant reactions associated with the charge-transfer resistance and double-layer capacitance at the electrodes and the other represents the long time-constant diffusional processes respectively.

B. Open-Circuit Voltage Estimation

The OCV is defined as the battery’s terminal voltage that is measured after a very long period of zero-current relaxation. Depending on the chemistry of electrodes, lithium-ion batteries may take up to several days to reach a final equilibrium potential. However, for practicality, the OCV at a particular SOC is generally measured based on the first few hours of load disconnection.

Herein, a pulsed-current test, similar to that reported in [8], is conducted at 25 °C to extract the charge and discharge OCV curves as a function of SOC. The results for the NMC test cell are presented in Fig. 4. Note that as the SOC moves downwards, the difference between the OCV values obtained for charge and discharge increases slightly. This phenomenon is referred to as hysteresis [9]. Since the measured hysteresis level for the test cell used here is not too large, it can be safely neglected in this work. For most energy storage applications with regenerative currents, the battery’s SOC is usually confined to a useable operating range of ~20 to 80%. Over this range, a 3rd order polynomial can be used to describe the average OCV-SOC relationship for a NMC battery cell.

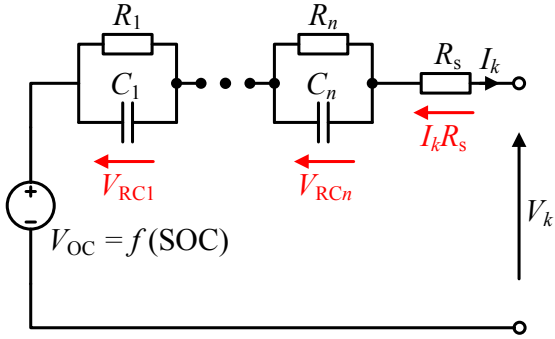


Fig. 3. Randles' equivalent-circuit model with n RC branches

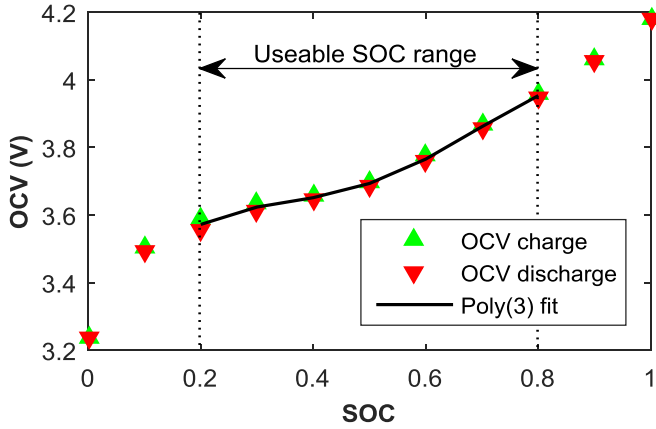


Fig. 4. OCV-SOC relationship for charge and discharge, showing 3rd order polynomial curve-fit over the useable SOC range of 20 to 80%

IV. PROPOSED HYBRID BATTERY IDENTIFICATION CONCEPT

In this paper, a hybrid battery parameter identification concept (see Fig. 5) is proposed as follows. The battery model parameters $\{R_s, R_1, C_1, R_2, C_2\}$ are initially identified using the PRBS method. For that, the excitation signal must be carefully designed. A no-load relaxation period of at least 30 minutes is necessary to ensure that the battery has reached a steady state. Thereafter, the model parameters are recursively updated through the dual-EKF algorithm [8] to account for any SOC-and/or temperature-induced variations in real time. Should the battery experience severe changes in operating conditions, the PRBS identification method can be re-applied.

A. Dual Extended Kalman Filter Theory

In general, a random process to be estimated using the dual-EKF algorithm can be modelled in the form,

$$\begin{aligned} \mathbf{x}_{k+1} &= f(\mathbf{x}_k, \mathbf{u}_k, \boldsymbol{\theta}_k) + \mathbf{w}_k \\ \mathbf{y}_k &= h(\mathbf{x}_k, \mathbf{u}_k, \boldsymbol{\theta}_k) + \mathbf{v}_k \\ \mathbf{w}_k &\sim N(0, \mathbf{Q}_k^x) \\ \mathbf{v}_k &\sim N(0, \mathbf{R}_k^x) \end{aligned} \quad (3)$$

where $\mathbf{x}_k \in \mathbb{R}^n$ is a vector containing the states to be predicted, $\boldsymbol{\theta}_k \in \mathbb{R}^q$ contains the time-varying model parameters, $\mathbf{u}_k \in \mathbb{R}^p$ is the exogenous model input, $\mathbf{y}_k \in \mathbb{R}^m$ is the output and

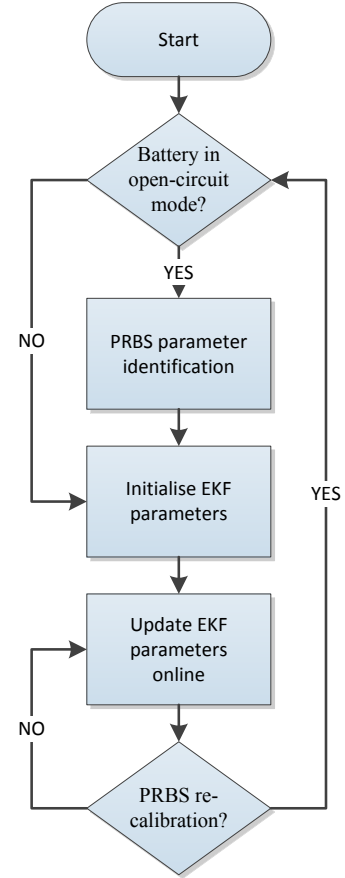


Fig. 5. Block diagram illustrating the proposed hybrid battery parameter identification concept

$\mathbf{w}_k \in \mathbb{R}^n$ and $\mathbf{v}_k \in \mathbb{R}^m$ are the zero-mean process and measurement noises of covariance \mathbf{Q}_k^x and \mathbf{R}_k^x respectively. The non-linear function $f(\cdot, \cdot)$ relates the states estimated at discrete time $k - 1$ to the states at the current time step k and $h(\cdot, \cdot)$ maps the updated states to the measurements taken at time step k .

Similarly, assuming that the model parameters vary slowly over time (i.e. minutes to hours), a second EKF can be designed to adaptively estimate the time-varying non-linear model parameters in real time. Thus, the equations for the EKF parameter estimator can be given as,

$$\begin{aligned} \boldsymbol{\theta}_{k+1} &= \boldsymbol{\theta}_k + \mathbf{r}_k \\ \mathbf{d}_k &= h(\mathbf{x}_k, \mathbf{u}_k, \boldsymbol{\theta}_k) + \mathbf{e}_k \\ \mathbf{r}_k &\sim N(0, \mathbf{Q}_k^\theta) \\ \mathbf{e}_k &\sim N(0, \mathbf{R}_k^\theta) \end{aligned} \quad (4)$$

where the dynamics of changes in parameters vector $\boldsymbol{\theta}_k$ are attributed to a small “imaginary” white noise $\mathbf{r}_k \in \mathbb{R}^p$ of covariance \mathbf{Q}_k^θ that evolves the parameters over time. The output equation $\mathbf{d}_k \in \mathbb{R}^m$ is given as a measurable function of $\boldsymbol{\theta}_k$ and a white noise $\mathbf{e}_k \in \mathbb{R}^m$ of covariance \mathbf{R}_k^θ to account for the measurement uncertainties. Thereafter, the algorithm performs three steps as follows.

I) Initialisation

At time-step $k = 0$, the states, parameters and the associated error covariance matrices are set to their best-guess values as per (5).

$$\begin{aligned}\hat{\mathbf{x}}_0^+ &= E[\mathbf{x}_0], \quad \mathbf{P}_{\mathbf{x},0}^+ = E[(\mathbf{x} - \hat{\mathbf{x}}_0^+)(\mathbf{x} - \hat{\mathbf{x}}_0^+)^T] \\ \hat{\boldsymbol{\theta}}_0^+ &= E[\boldsymbol{\theta}_0], \quad \mathbf{P}_{\boldsymbol{\theta},0}^+ = E[(\boldsymbol{\theta} - \hat{\boldsymbol{\theta}}_0^+)(\boldsymbol{\theta} - \hat{\boldsymbol{\theta}}_0^+)^T]\end{aligned}\quad (5)$$

2) Time-update

At this step, the algorithm updates the state and parameter estimates $\hat{\mathbf{x}}_k^-$ and $\hat{\boldsymbol{\theta}}_k^-$ and their corresponding error covariance $\mathbf{P}_{\mathbf{x},k}^-$ and $\mathbf{P}_{\boldsymbol{\theta},k}^-$ respectively. The subsequent time-update equations for the state and parameter EKFs are expressed by (10) and (11).

$$\begin{aligned}\hat{\mathbf{x}}_k^- &= f(\hat{\mathbf{x}}_{k-1}^+, \mathbf{u}_{k-1}, \hat{\boldsymbol{\theta}}_k^-) \\ \mathbf{P}_{\mathbf{x},k}^- &= \mathbf{F}_{k-1} \mathbf{P}_{\mathbf{x},k-1}^- \mathbf{F}_{k-1}^T + \mathbf{Q}_k^x \\ \mathbf{F}_{k-1} &= \left. \frac{\partial f(\hat{\mathbf{x}}_{k-1}^+, \mathbf{u}_{k-1}, \hat{\boldsymbol{\theta}}_k^-)}{\partial \mathbf{x}_{k-1}} \right|_{\mathbf{x}_{k-1} = \hat{\mathbf{x}}_{k-1}^+}\end{aligned}\quad (6)$$

$$\begin{aligned}\hat{\boldsymbol{\theta}}_k^- &= \hat{\boldsymbol{\theta}}_{k-1}^+ \\ \mathbf{P}_{\boldsymbol{\theta},k}^- &= \mathbf{P}_{\boldsymbol{\theta},k-1}^+ + \mathbf{Q}_k^\theta\end{aligned}\quad (7)$$

where, the “super minus” notation indicates that this is the best (*a priori*) estimate available prior to assimilating the measurements at time step k . \mathbf{F}_{k-1} denotes the Jacobian matrix of partial derivatives of $f(\cdot, \cdot)$ with respect to model states.

3) Measurement-update

After a measurement has been taken at time step k , both EKFs take this into consideration to update the state $\hat{\mathbf{x}}_k^+$ and parameter $\hat{\boldsymbol{\theta}}_k^+$ estimates and their corresponding error covariance as $\mathbf{P}_{\mathbf{x},k}^+$ and $\mathbf{P}_{\boldsymbol{\theta},k}^+$ respectively.

$$\begin{aligned}\mathbf{L}_k^x &= \mathbf{P}_{\mathbf{x},k}^-(\mathbf{H}_k^x)^T [\mathbf{H}_k^x \mathbf{P}_{\mathbf{x},k}^-(\mathbf{H}_k^x)^T + \mathbf{R}_k^x]^{-1} \\ \hat{\mathbf{x}}_k^+ &= \hat{\mathbf{x}}_k^- + \mathbf{L}_k^x [\mathbf{y}_k - h(\hat{\mathbf{x}}_k^-, \mathbf{u}_k, \hat{\boldsymbol{\theta}}_k^-)] \\ \mathbf{P}_{\mathbf{x},k}^+ &= (\mathbf{I} - \mathbf{L}_k^x \mathbf{H}_k^x) \mathbf{P}_{\mathbf{x},k}^- (\mathbf{I} - \mathbf{L}_k^x \mathbf{H}_k^x)^T + \mathbf{L}_k^x \mathbf{R}_k^x (\mathbf{L}_k^x)^T \\ \mathbf{H}_k^x &= \left. \frac{\partial h(\mathbf{x}_k, \mathbf{u}_k, \hat{\boldsymbol{\theta}}_k^-)}{\partial \mathbf{x}_k} \right|_{\mathbf{x}_k = \hat{\mathbf{x}}_k^-}\end{aligned}\quad (8)$$

$$\begin{aligned}\mathbf{L}_k^\theta &= \mathbf{P}_{\boldsymbol{\theta},k}^-(\mathbf{H}_k^\theta)^T [\mathbf{H}_k^\theta \mathbf{P}_{\boldsymbol{\theta},k}^-(\mathbf{H}_k^\theta)^T + \mathbf{R}_k^\theta]^{-1} \\ \hat{\boldsymbol{\theta}}_k^+ &= \hat{\boldsymbol{\theta}}_k^- + \mathbf{L}_k^\theta [\mathbf{d}_k - h(\hat{\mathbf{x}}_k^-, \mathbf{u}_k, \hat{\boldsymbol{\theta}}_k^-)] \\ \mathbf{P}_{\boldsymbol{\theta},k}^+ &= (\mathbf{I} - \mathbf{L}_k^\theta \mathbf{H}_k^\theta) \mathbf{P}_{\boldsymbol{\theta},k}^- (\mathbf{I} - \mathbf{L}_k^\theta \mathbf{H}_k^\theta)^T + \mathbf{L}_k^\theta \mathbf{R}_k^\theta (\mathbf{L}_k^\theta)^T \\ \mathbf{H}_k^\theta &= \left. \frac{\partial h(\hat{\mathbf{x}}_k^-, \mathbf{u}_k, \boldsymbol{\theta}_k)}{\partial \boldsymbol{\theta}_k} \right|_{\boldsymbol{\theta}_k = \hat{\boldsymbol{\theta}}_k^-}\end{aligned}\quad (9)$$

where \mathbf{L}_k^x and \mathbf{L}_k^θ are the Kalman gain matrices and \mathbf{H}_k^x and \mathbf{H}_k^θ represent the Jacobians of the nonlinear function $h(\cdot, \cdot)$ with respect to model states and parameters.

B. Generation of PRBS Excitation Signal

When designing a PRBS signal, there are two base parameters that must be carefully selected [10]. These include the source clock frequency (f_{clk}) and the number of shift registers (b), which in turn define the PRBS frequency bandwidth and the test duration in seconds.

Therefore, a theoretical analysis is conducted to determine f_{clk} and n for the battery identification problem in hand. For a maximum-length PRBS, the test duration T_{prbs} can be defined as,

$$T_{\text{prbs}} = \frac{N}{f_{\text{clk}}}\quad (10)$$

where $N = 2^b - 1$ is the sequence length and b is the PRBS bit-length.

Through the analysis of the signal’s power spectral density (PSD), the bandwidth over which the PRBS data is useable can be realised [11]. Fig. 6 presents the PSD for an exemplary 4-bit 10 Hz PRBS, where the power spectrum is represented by discrete power points separated by f_{clk}/N . As can be observed, the corresponding PSD has a *sinc* function characteristic, which can be described by (11).

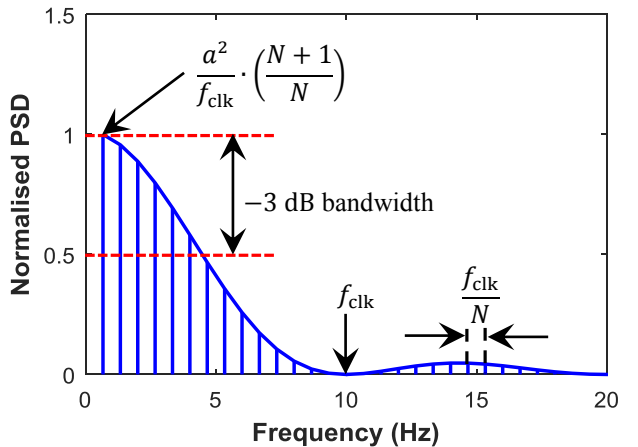


Fig. 6. Power spectral density for a 4-bit 10 Hz PRBS

$$S_{xx}(f) = \frac{a^2(N+1)}{N \cdot f_{\text{clk}}} \left[\frac{\sin(f\pi/f_{\text{clk}})}{f\pi/f_{\text{clk}}} \right]^2.\quad (11)$$

The band-limit of a PRBS is defined by the frequency at which its power is attenuated by -3 dB (i.e. when power drops by half). This event occurs when,

$$\left[\frac{\sin(f\pi/f_{\text{clk}})}{f\pi/f_{\text{clk}}} \right]^2 = 0.5 \Rightarrow f_{\max} \approx \frac{f_{\text{clk}}}{2.25}.\quad (12)$$

Now, considering the lower band-limit as $f_{\min} = f_{\text{clk}}/N$ and using f_{\max} from (12), the frequency band (f_{band}) over which the PRBS information are useful can be established.

$$f_{\text{band}} = f_{\text{clk}} \left(\frac{1}{2.25} - \frac{1}{N} \right) \quad (13)$$

$$f_{\text{norm}} = \frac{f_{\text{band}}}{f_{\text{max}}} = 1 - \frac{2.25}{N}$$

where f_{norm} is the normalised frequency band.

Using the EIS analyser configured in Fig. 2 and a testing procedure similar to that reported in [4], the impedance of the NMC test cell was measured over a frequency range of 5 mHz to 5 kHz. The test was carried out in steps of $\Delta \text{SOC} = 10\%$ over the range of 0 to 100%. The effect of temperature was also considered by performing EIS tests at five different temperature settings of 5, 15, 25, 35 and 45 °C.

As can be observed in Fig. 7, there exists an increasing trend in the measured impedance with decreasing SOC and temperature. This effect is more predominant towards the lower end of spectrum (i.e. $f < 5$ Hz), where diffusional impedance [4] occurs. This particular element conveys vital information on the battery's main charge storage and can serve not only as a good indicator for SOP and SOF, but also as an online battery health monitor [12].

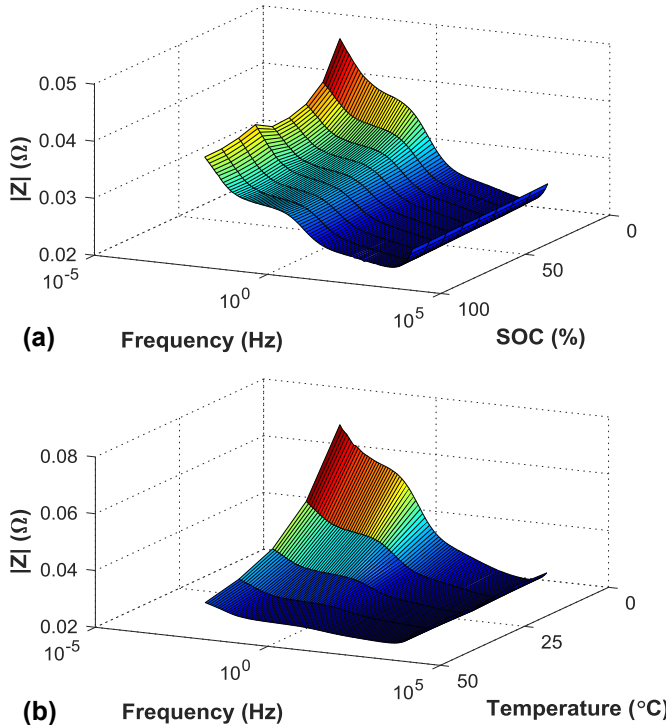


Fig. 7. Impedance magnitude as a function of (a) battery SOC and (b) operating temperature for 3.6 Ah NMC test cell

According to (13), a PRBS clock frequency of $f_{\text{clk}} = 11.25$ Hz should be sufficient to capture the battery's diffusional dynamics over the frequency band of $5 \text{ mHz} < f < 5 \text{ Hz}$. However, to be able to use the Maccor battery tester as a PRBS excitation and acquisition device, a clock frequency of $f_{\text{clk}} = 10$ Hz is chosen herein, yielding a maximum frequency band-limit of 4.44 Hz.

In order to maintain the white-noise-like properties of the generated PRBS and to avoid spectral leakage during analysis, the sequence must be captured as a whole. This leads to the consideration for the required PRBS bit-length, which in turn dictates the test duration. In this paper, a bit-length of $b = 10$ is chosen as a trade-off, leading to a PRBS perturbation signal that is conveniently less than two minutes long and covers a frequency range of $0.01 \text{ Hz} \leq f \leq 4.44 \text{ Hz}$.

V. RESULTS AND DISCUSSION

To verify the proposed battery parameter identification method, two tests are devised. First, the NMC cell is applied with the generated 10-bit 10 Hz PRBS at $\Delta \text{SOC} = 10\%$. Intervals. A 0.5 C current level is used to move SOC downwards and a one-hour relaxation period is allowed prior to PRBS excitation. The purpose of this test is to evaluate the accuracy of the PRBS parameter identification compared to the more precise EIS method. A section of the measured battery voltage and current are shown in Fig. 8(a) and (b) respectively.

Second, a test profile based on the Artemis drive cycle [13] is derived to dynamically discharge the test cell from 80 to 20% SOC. A single repetition of this cycle is given in Fig. 8(c). This test is carried out to verify the performance of the DEKF algorithm for both parameters and SOC estimation. The parameters EKF is initialised with the PRBS-obtained parameters at SOC = 80%. Moreover, the states EKF is incorrectly set with SOC = 20%, whilst true SOC = 79.2%.

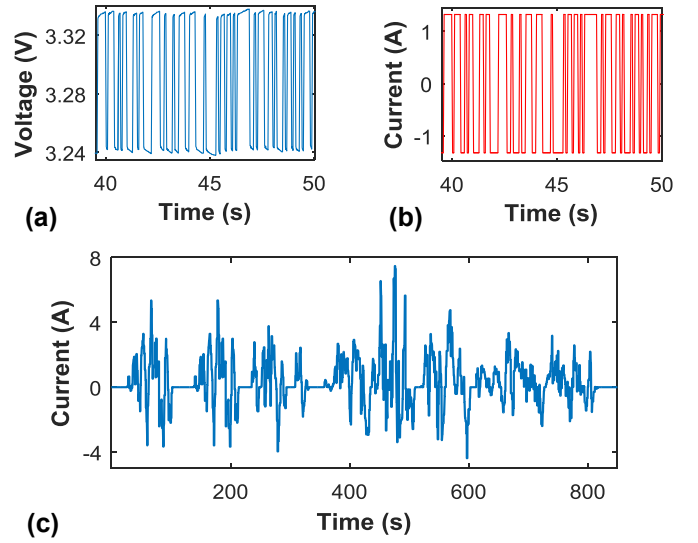


Fig. 8. Section of measured PRBS (a) voltage and (b) current, and (c) single repetition of Artemis [13] cycle

An offline non-linear least-squares method as described in [4] is used here to extract the battery parameters from the EIS- and PRBS-obtained complex impedance data. Fig. 9 presents the model parameters identified as a function of SOC using EIS, PRBS and the proposed hybrid-DEKF method. The results obtained using the inexpensive PRBS approach are in good agreement with the more precise and laboratory-based EIS method. This further proves the validity of the PRBS method for online battery characterisation and monitoring purposes.

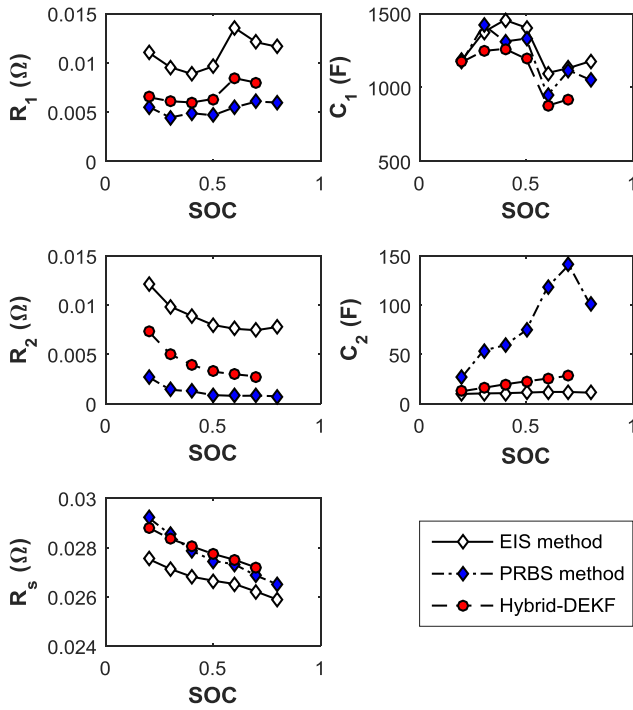


Fig. 9. Comparison of 2-RC model parameters identified using EIS, PRBS and proposed hybrid-DEKF method

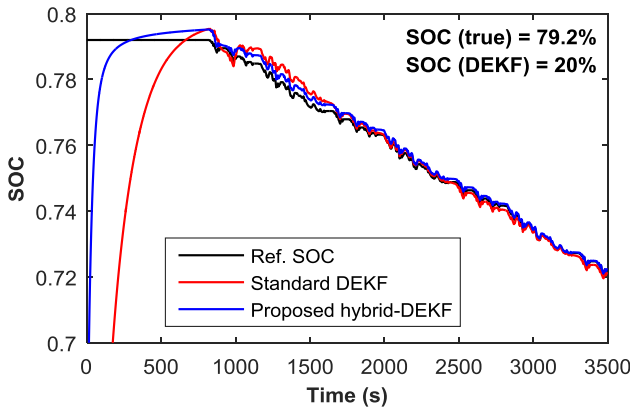


Fig. 10. Comparison of estimated SOC using standard DEKF and proposed hybrid-DEKF method

The DEKF's identification performance is also demonstrated in Fig. 9, where the SOC filter is allowed to fully converge before the first set of estimated parameters are recorded at SOC = 70%. After correct initialisation of the parameters vector using PRBS, the DEKF algorithm effectively deals with the SOC-induced variations in model parameters. The SOC convergence of the hybrid-DEKF algorithm for part of the multi-cycle Artemis test profile is presented in Fig. 10. As can be seen, the proposed estimator benefits from a faster convergence time of ~200 seconds. It should be noted that for the standard DEKF, the initial parameters are set arbitrarily as $R_s = 0.02$, $R_1 = 0.01$, $C_1 = 1000$, $R_2 = 0.01$ and $C_2 = 100$.

VI. CONCLUSIONS

For most *in situ* applications, such as in EVs and grid-tie energy storage, the battery model parameters need to be identified in real time. Difficulty arises when the input/output signals are not persistently exciting, which can result in divergence and failure of the incorporated BMS. In practice, the DEKF algorithm seems to cope well with the lack of persistence of excitation, if and only if the parameters EKF is initialised reasonably correct. In this paper, a hybrid parameter identification technique was proposed that comprised of a PRBS excitation signal, which was used to correctly initialise the battery parameters. Thereafter, the DEKF algorithm was implemented recursively to adapt the parameters with respect to SOC modifications. The PRBS- and DEKF-identified parameters were in good agreement with the EIS method.

REFERENCES

- [1] H. Rahimi-Eichi, F. Baronti, and M.-Y. Chow, "Online Adaptive Parameter Identification and State-of-Charge Coestimation for Lithium-Polymer Battery Cells," *Ind. Electron. IEEE Trans.*, vol. 61, no. 4, pp. 2053–2061, Apr. 2014.
- [2] D. Andre, C. Appel, T. Soczka-Guth, and D. U. Sauer, "Advanced mathematical methods of SOC and SOH estimation for lithium-ion batteries," *J. Power Sources*, vol. 224, pp. 20–27, 2013.
- [3] R. Morello, W. Zamboni, F. Baronti, R. Di Renzo, R. Roncella, G. Spagnuolo, and R. Saletti, "Comparison of state and parameter estimators for electric vehicle batteries," in *Industrial Electronics Society, IECON 2015 - 41st Annual Conference of the IEEE*, 2015, pp. 5433–5438.
- [4] S. Nejad, D. T. Gladwin, and D. A. Stone, "Sensitivity of lumped parameter battery models to constituent parallel-RC element parameterisation error," in *Industrial Electronics Society, IECON 2014 - 40th Annual Conference of the IEEE*, 2014, pp. 5660–5665.
- [5] V. V Chalam, *Adaptive Control Systems: Techniques and Applications*. New York: Marcel Dekker, Inc., 1987.
- [6] C. R. Gould, C. M. Bingham, D. A. Stone, and P. Bentley, "New battery model and state-of-health determination through subspace parameter estimation and state-observer techniques," *IEEE Trans. Veh. Technol.*, vol. 58, no. 8, pp. 3905–3916, Oct. 2009.
- [7] S. Nejad, D. T. Gladwin, and D. A. Stone, "A systematic review of lumped-parameter equivalent circuit models for real-time estimation of lithium-ion battery states," *J. Power Sources*, vol. 316, pp. 183–196, 2016.
- [8] S. Nejad, D. T. Gladwin, and D. A. Stone, "Enhanced state-of-charge estimation for lithium-ion iron phosphate cells with flat open-circuit voltage curves," in *Industrial Electronics Society, IECON 2015 - 41st Annual Conference of the IEEE*, 2015, pp. 3187–3192.
- [9] M. S. R. Khatib, A.L. Dalverny and M. L. D. M. Gabersek, "Origin of the Voltage Hysteresis in the CoP Conversion Material for Li-Ion Batteries," *J. Phys. Chem.*, vol. 117, no. 2, pp. 837–849, 2013.
- [10] A. J. Fairweather, M. P. Foster, and D. A. Stone, "Modelling of VRLA batteries over operational temperature range using pseudo random binary sequences," *J. Power Sources*, vol. 207, pp. 56–59, Jun. 2012.
- [11] J. N. Davidson, D. A. Stone, M. P. Foster, and D. T. Gladwin, "Improved Bandwidth and Noise Resilience in Thermal Impedance Spectroscopy by Mixing PRBS Signals," *IEEE Trans. Power Electron.*, vol. 29, no. 9, pp. 4817–4828, 2014.
- [12] D. I. Stroe, M. Swierczynski, A. I. Stan, V. Knap, R. Teodorescu, and S. J. Andreasen, "Diagnosis of lithium-ion batteries state-of-health based on electrochemical impedance spectroscopy technique," in *Energy Conversion Congress and Exposition (ECCE), 2014 IEEE*, 2014, pp. 4576–4582.
- [13] T. Barlow, S. Latham, I. McCrae, and P. Boulter, "A reference book of driving cycles for use in the measurement of road vehicle emissions," 2009.